Theoretical analysis and computer simulation of dynamic processes for a driven diffusive two-lane system

Qing-Yi Hao,[1,2,*] Rui Jiang,[3,†] Chao-Yun Wu,[1,4] Ning Guo,[5] Bing-Bing Liu,[1,6] and Yunxin Zhang[2]
[1]*School of Mathematics and Computational Science, Anqing Normal University, Anqing 246133, China*
[2]*School of Mathematical Sciences, Fudan University, Shanghai 200433, China*
[3]*MOE Key Laboratory for Urban Transportation Complex Systems Theory and Technology, Beijing Jiaotong University, Beijing 100044, China*
[4]*School of Engineering Science, University of Science and Technology of China, Hefei 230026, China*
[5]*School of Automotive and Transportation Engineering, Hefei University of Technology, Hefei 230009, China*
[6]*School of Management, University of Science and Technology of China, Hefei 230026, China*

(Received 9 July 2018; published 10 December 2018)

The driven diffusive system is a powerful tool to investigate properties of nonequilibrium state statistical physics, vehicle traffic, and biological transport systems. This paper presents a two-channel asymmetric exclusion process model, in which collective dynamics with interactions of particles between two lanes are considered. Computer simulation and mean-field analysis are carried out to calculate the flow rate under periodic boundary. On the whole, the results from the two-vertical-horizontal-cluster mean-field method are in good agreement with the simulation results. Two types of phases including double peaked and single peaked appear in the flow rate of the system. Based on investigating the coarsening process of the system, one can get a conjecture that the system is homogeneous when the critical density at which normalized residence distribution turns into nonmonotonous variability from monotonous decrease equals 0.5. These findings may be helpful to deeply understand the dynamic features of nonequilibrium state systems and traffic or transport systems.

DOI: 10.1103/PhysRevE.98.062111

I. INTRODUCTION

Driven diffusive systems, due to their simple rules and rich dynamic features, are payed close attention to in various fields including, but not limited to, physics [1], biology [2,3], surface growth [4], polymer dynamics in dense media [5], diffusion through membrane channels [6], fast ionic conductors [7], and traffic [8]. Especially, they have become basic and critical tools to investigate properties of the systems far from thermal equilibrium [1] and biological transport systems [9,10].

The most prominent paradigm of driven diffusive systems is the totally asymmetric exclusion process (TASEP) proposed originally by MacDonald and Gibbs to model the motion of multiple ribosomes along a mRNA strand during protein synthesis inside living cells [11,12]. Hereafter, numerous variants of the TASEP have been developed [8,9,13]. Some of these extended TASEP models are considered in single-channel systems, some are investigated in two-channel or multiple-channel systems [14–17]. Thereinto, collective dynamics with interactions of particle transport were studied in single-channel systems [18–20]. There are some investigations focusing on interactions between particles on different lanes in two-channel systems [21–25]. However, the impacts of various interactions on the transport of particles such as molecular motors, pedestrians, and vehicles have not been fully explored in two-channel systems. Especially, the interaction between particles in two lanes is rarely studied in the two-channel system without lane changing.

Besides computer simulation, mean-field analysis is also one powerful tool in investigating driven diffusive systems. Usually, the mean-field method includes simple mean field and cluster mean field [8]. The simple mean field ignores completely correlations and the cluster mean field takes into account some correlations in the system. So mean-field analysis is an approximate method to study the systems owning correlations under normal conditions. Except for the original TASEP model with no correlation [26] and few TASEP models owning correlations [27,28], the exact solution of most TASEP models can barely be obtained by mean-field analysis. Considering interactions of particles in one lane, the horizontal cluster mean-field method can be employed. But vertical cluster mean field should be used if the interactions of particles in different lanes are investigated in two or multiple channel systems [16,21,22].

In this paper, a two-channel TASEP model is proposed. In the model, the interaction between particles in two lanes without lane changing is studied, and the attractive and repulsive effect of particles in different lanes is considered. Computer simulation and mean-field analysis are carried out to calculate the flow rate under periodic boundary. Double-peaked and single-peaked properties are found in the curves of flow rate with different model parameters p and q. The results from the two-vertical-horizontal-cluster mean-field method (CMF) are in good agreement with the results from computer simulation. Through investigating the coarsening process of

*haoqy@aqnu.edu.cn
†jiangrui@bjtu.edu.cn

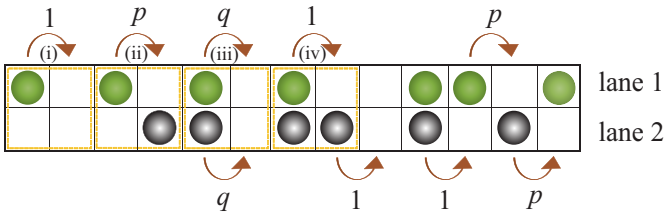

FIG. 1. Schematic illustration of the two-lane TASEP model. Blue full circle indicates the particle in upper lane (lane 1), white and black radial indicates the particle in lower lane (lane 2). The top and bottom boundaries are closed. The left and right boundaries are periodic. The four configurations marked with yellow dashed boxes denote the four cases of particle hopping in our model for lane 1, and similar cases for lane 2.

the system based on Monte Carlo simulation, we find that the normalized residence distribution $p(s)$ is monotonically decreasing when the density is under a critical density ρ_c, and $p(s)$ is nonmonotonic when the density is above the ρ_c. Interestingly, the ρ_c influences the accuracy of the CMF result. In view of this, we present a speculation that the system is homogeneous when the critical density $\rho_c = 0.5$.

The paper is organized as follows. The model is described in Sec. II. Simulation results and mean-field analysis are presented in Sec. III. Finally, we give conclusions in Sec. V.

II. MODEL

The model is composed of two lanes. It is defined in a $2 \times L$ lattice; each site can be either empty, or occupied by a single particle. In each lane, a particle can move to the right along the same lane according to some probability, but particles are forbidden to change lanes. The transition probability is not only related to the state of the next site in each lane, but is also related to the state of neighbor sites in the other lane. Here, the random update rule is employed. As shown in Fig. 1, the hopping rule of the particle in this TASEP model is as follows. If a particle in site i is chosen to update,

(i) if the right neighboring site $i+1$ is occupied, the particle stays at its site i;

(ii) if the right neighboring site $i+1$ is empty;

(a) if the site i and $i+1$ in the other lane are both empty, the particle will hop forward to the right neighboring site $i+1$ at rate 1[case (i) in Fig. 1];

(b) if the site i is empty and site $i+1$ is occupied in the other lane, the particle will hop forward to the right neighboring site $i+1$ at rate p [case (ii) in Fig. 1];

(c) if the site i in the other lane is occupied and the site $i+1$ in the other lane is empty, the particle will hop forward to the right neighboring site $i+1$ at rate q [case (iii) in Fig. 1];

(d) if the site i and $i+1$ in the other lane are occupied, the particle will hop forward to the right neighboring site $i+1$ at rate 1 [case (iv) in Fig. 1].

When $p = q = 1$, the model reduces to the standard TASEP model. This model rule can be regarded as the motivation of biological transport [22], pedestrian flow, or vehicle traffic flow [21,24]. Though changing lanes is not occurring, the movement of a molecular motor (pedestrian, vehicle) in one lane often is affected by that in the adjacent lane. For instance, in vehicle traffic flow, considering safety, the driver in lane 1 may slow down in case (ii) and speed up in case (iii) as shown in Fig. 1. Under pedestrian traffic conditions, in case (ii), the pedestrian in lane 1 may move forward with a big rate to catch up with the acquaintance or friend in lane 2, otherwise, the pedestrian in lane 1 may move forward with a small rate to keep away from the stranger in lane 2. Similarly, in case (iii), the pedestrian in lane 1 may move forward with a small rate to keep side by side with the acquaintance or friend in lane 2, otherwise, the pedestrian in lane 1 may move forward with a big rate to surpass the stranger in lane 2. In cases (i) and (iv), the states of two neighbor sites in the other lane (lane 2) are the same, that is, both are empty or occupied, so the hopping rates are set to 1 for simplicity.

III. MEAN-FIELD ANALYSIS AND SIMULATION

This section carries out mean-field analysis and Monte Carlo simulations for the model. The density ρ of each lane is set to be equal; here the density ρ is defined as particle numbers in one lane divided by L. In the Monte Carlo simulations, random initial distributions are employed.

A. Simple mean-field method

Ignoring correlations, we analyze the current of system by the simple mean-field method (SMF). We investigate the four probabilities P_0, P_1, P_2, P_3 corresponding to four vertical cluster configurations 0, 1, 2, and 3 as shown in Fig. 2(a). Obviously, according to the conservation of probability, one can get

$$P_0 + P_1 + P_2 + P_3 = 1. \tag{1}$$

Moreover, the definition of density gives

$$P_1 + P_3 = \rho \tag{2}$$

and

$$P_2 + P_3 = \rho. \tag{3}$$

The evolution of four probabilities can be described with master equations according to the configuration in Fig. 3(a). Specifically, for P_1, the master equation is

$$\begin{aligned}\frac{dP_1}{dt} &= P_3P_0q + P_3P_0q + P_3P_1 + P_1P_0 \\ &\quad - P_1P_2p - P_2P_1p - P_3P_1 - P_1P_0.\end{aligned} \tag{4}$$

When the system reaches a stationary state, $\frac{dP_1}{dt} = 0$. Thus

$$pP_1P_2 = qP_0P_3. \tag{5}$$

Substituting (1)–(3) into (5), we obtain

$$(q-p)P_3^2 + (q + 2p\rho - 2q\rho)P_3 - p\rho^2 = 0. \tag{6}$$

Solving Eq. (6), we get the solution

$$P_3 = \begin{cases} \frac{2q\rho - q - 2p\rho + \sqrt{4p(q-p)\rho^2 + (q+2p\rho-2q\rho)^2}}{2(q-p)}, & p \neq q, \\ \rho^2, & p = q. \end{cases} \tag{7}$$

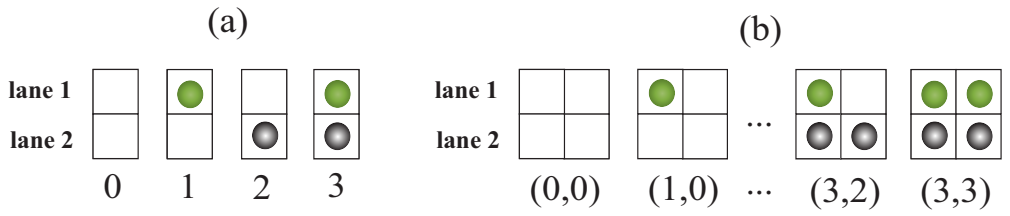

FIG. 2. Possible configurations of a vertical cluster for (a) simple mean field (four configurations) and (b) two-cluster mean field (16 configurations, here only partly listed). The number labeled below vertical cluster indicates the type of the vertical cluster.

Substituting (7) into (1)–(3), P_0, P_1, P_2 can be calculated respectively. Consequently, the currents on lanes 1 and 2 are

$$J_1 = P_1P_0 + P_3P_2 + P_1P_2p + P_3P_0q \tag{8}$$

and

$$J_2 = P_2P_0 + P_3P_1 + P_2P_1p + P_3P_0q. \tag{9}$$

From Eqs. (2) and (3), we have $P_1 = P_2$. Therefore, the currents on lanes 1 and 2 are equal, i.e., $J_1 = J_2$. In the case of $p \neq q$, the expression of current is

$$\begin{aligned} J = {} & \frac{1}{2(p-q)^2}((p+q-2pq) \\ & \times \sqrt{q[q(1-2\rho)^2 - 4p(\rho-1)\rho]} \\ & + pq[4\rho(p+\rho-p\rho-1)-1] \\ & + q^2\{p[2+4(\rho-1)\rho] - (1-2\rho)^2\}), \end{aligned} \tag{10}$$

and in the case of $p = q$, the expression of flow rate is

$$J = \rho + (2p-3)\rho^2 + (4-4p)\rho^3 + (2p-2)\rho^4. \tag{11}$$

B. Cluster mean-field method

To consider the correlation between particles, now we use the cluster mean-field method. Here we define an n cluster to be a collection of n successive vertical clusters, and use $P(\sigma_1, \sigma_2, \ldots, \sigma_n)$ to denote the probability of finding an n cluster in the state $(\sigma_1, \sigma_2, \ldots, \sigma_n)$ under the steady state of the system. Taking into account that hop rates in the model only depend on the states of two adjacent vertical clusters, we only carry out two-cluster mean-field analysis. In this case, the state of the two-cluster (σ_i, σ_{i+1}) at time $t+1$ depends on the state of the three-cluster $(\sigma_{i-1}, \sigma_i, \sigma_{i+1})$ or $(\sigma_i, \sigma_{i+1}, \sigma_{i+2})$ at time t as shown in Fig. 3(b). Here the $\sigma_i = 0, 1, 2, 3$, corresponds to the four states shown in Fig. 2(a), respectively.

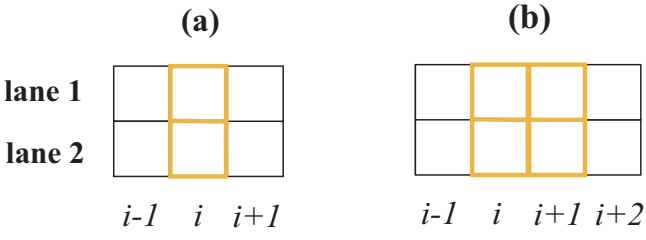

FIG. 3. Site configurations to be considered in (a) simple mean field (SMF) analysis and (b) two-cluster mean field (CMF) analysis. The thick orange box indicates the target vertical cluster to be considered.

So there are 16 two-cluster probabilities $P(\sigma_i, \sigma_{i+1})$ to be solved. Figure 4 shows the configurations of three-cluster probabilities (1,2,3), (2,1,0). To make a distinction between three-cluster $(\sigma_{i-1}, \sigma_i, \sigma_{i+1})$ and $(\sigma_i, \sigma_{i+1}, \sigma_{i+2})$, we add a line under σ_i and σ_{i+1} in the following expressions. For example, three-cluster probabilities $P(1, 2, 3)$ and $P(2, 1, 0)$ corresponding to Fig. 4 can be denoted as $P(1, \underline{2, 3})$ and $P(\underline{2, 1}, 0)$, respectively.

According to cluster mean-field theory and our model rules, the master equation corresponding to the temporal evolution of two-cluster probability $P(0, 0)$ can be expressed as

$$\begin{aligned} \frac{dP(0,0)}{dt} = {} & P(\underline{0,1},0) + P(\underline{0,1},2)p + P(\underline{0,2},0) \\ & + P(\underline{0,2},1)p - P(1,\underline{0,0}) \\ & - P(2,\underline{0,0}) - 2P(3,\underline{0,0})q. \end{aligned} \tag{12}$$

In general n-cluster approximation, one divides the n cluster into "clusters" of length n such that two adjacent clusters have $n-1$ vertical clusters in common. In the two-cluster mean-field analysis, $P(\sigma_{i-1}, \sigma_i, \sigma_{i+1})$ and $P(\sigma_i, \sigma_{i+1}, \sigma_{i+2})$ can be expressed mathematically as

$$P(\sigma_{i-1}, \sigma_i, \sigma_{i+1}) = P(\sigma_{i-1}|\underline{\sigma_i})P(\sigma_i, \sigma_{i+1}), \tag{13}$$

and

$$P(\sigma_i, \sigma_{i+1}, \sigma_{i+2}) = P(\sigma_i, \sigma_{i+1})P(\underline{\sigma_{i+1}}|\sigma_{i+2}), \tag{14}$$

respectively, where

$$P(\sigma_{i-1}|\underline{\sigma_i}) = \frac{P(\sigma_{i-1}, \sigma_i)}{\sum_{\sigma_{i-1}} P(\sigma_{i-1}, \sigma_i)} \tag{15}$$

and

$$P(\underline{\sigma_{i+1}}|\sigma_{i+2}) = \frac{P(\sigma_{i+1}, \sigma_{i+2})}{\sum_{\sigma_{i+2}} P(\sigma_{i+1}, \sigma_{i+2})} \tag{16}$$

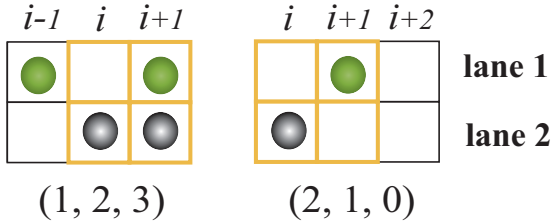

FIG. 4. Configurations sketch of three cluster (1,2,3), (2,1,0). The thick orange box indicates the target vertical cluster to be considered.

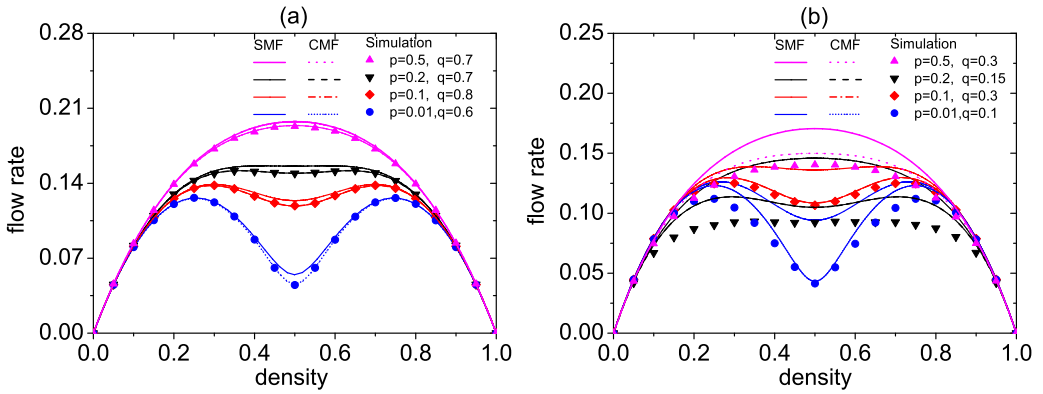

FIG. 5. Diagrams of current vs density ρ for (a) large values of q, and (b) small values of q. The symbol, solid line, and broken line present simulation result, simple mean-field result, and cluster mean-field analysis, respectively.

are two-cluster conditional probabilities. Applying Eqs. (13) and (14) to the three-cluster probabilities involved in the right-hand side of Eq. (12), and noting $\frac{dP(0,0)}{dt} = 0$ in the stationary state, Eq. (12) can be simplified as

$$\frac{P(0,1)P(1,0) + P(0,1)P(1,2)p}{P(1,0) + P(1,1) + P(1,2) + P(1,3)} + \frac{P(0,2)P(2,0) + P(0,2)P(2,1)p}{P(2,0) + P(2,1) + P(2,2) + P(2,3)} - \frac{P(1,0)P(0,0) + P(2,0)P(0,0) + 2P(3,0)P(0,0)q}{P(0,0) + P(1,0) + P(2,0) + P(3,0)} = 0. \quad (17)$$

According to the symmetry of the two lanes in the model, one can get the following six equations:

$$P(2,0) = P(1,0), \quad (18)$$

$$P(0,2) = P(0,1), \quad (19)$$

$$P(2,2) = P(1,1), \quad (20)$$

$$P(2,1) = P(1,2), \quad (21)$$

$$P(3,2) = P(3,1), \quad (22)$$

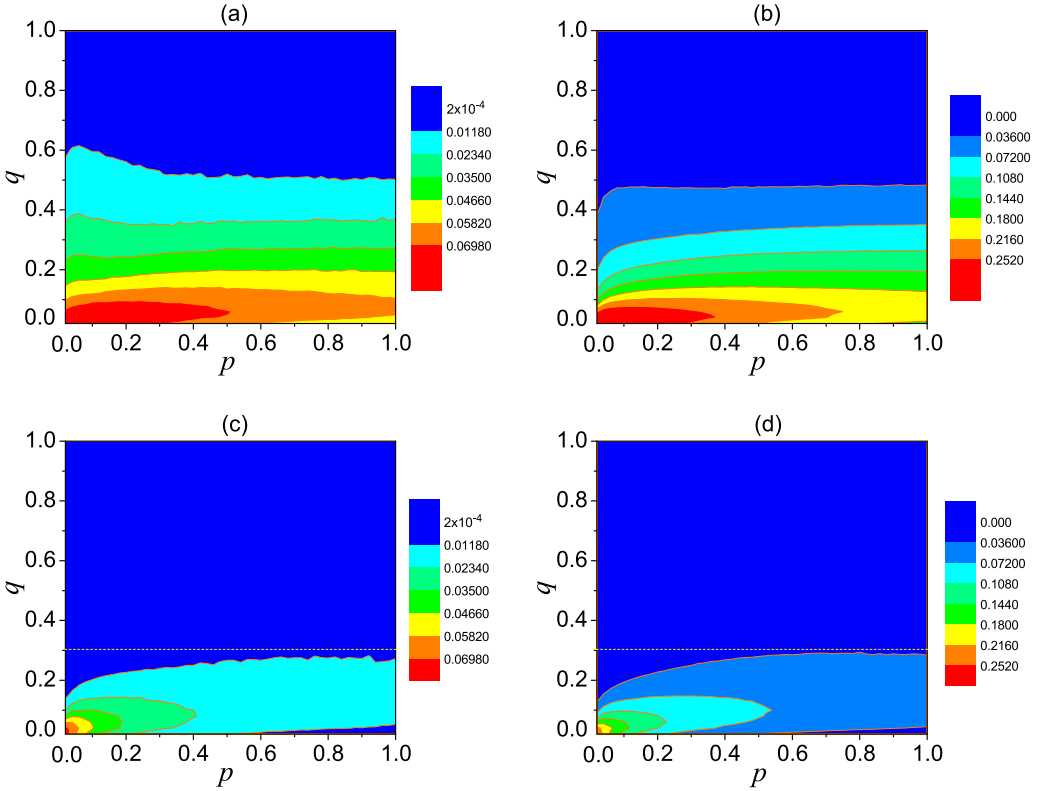

FIG. 6. Contours of current deviation of mean-field analysis from simulation. (a) Maximum deviation corresponding SMF, (b) mean square deviation corresponding SMF, (c) maximum deviation corresponding CMF, (d) mean square deviation corresponding CMF. The dashed line in (c) and (d) is a guide for eyes to observe and compare the contour in Fig. 12.

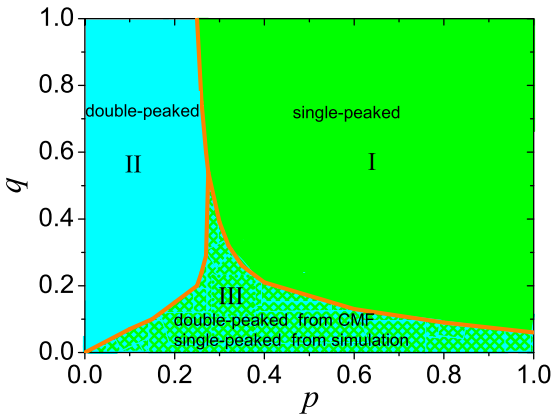

FIG. 7. Phase diagram. Boundary separating double-peaked from single-peaked current-density relation in (p, q) space; region I indicates single-peaked from CMF and simulation, region II denotes double-peaked from CMF and simulation, and region III indicates double-peaked from CMF, but single-peaked from simulation.

$$P(2, 3) = P(1, 3). \tag{23}$$

Moreover, the conservation of probability requires that

$$\sum_{i,j=0}^{3} P(i, j) = 1. \tag{24}$$

Furthermore, the definition of density gives

$$P(1, 0) + P(1, 1) + P(1, 2) + P(1, 3) + P(3, 0) + P(3, 1) + P(3, 2) + P(3, 3) = \rho. \tag{25}$$

To form closed equations about 16 variables $P(\sigma_i, \sigma_{i+1})$, we have to obtain seven other independent equations. According to the similar derivation of Eq. (17), we can get the seven independent equations shown in the Appendix [(A1)–(A7)].

It is difficult to get the analytical solutions of the nonlinear equations including (17)–(25) and (A1)–(A7). But numerical solutions could be obtained by the Newton iteration method. By the way, in this work, we compute the numerical solutions of nonlinear equations by the function *FindRoot* based on the Newton method in software *Mathematica* 10.3. After getting the numerical solutions of the 16 probabilities $P(\sigma_i, \sigma_{i+1})$, the current of the system can be calculated as

$$J = P(1, 0) + P(3, 2) + P(1, 2)p + P(3, 0)q, \tag{26}$$

or

$$J = P(2, 0) + P(3, 1) + P(2, 1)p + P(3, 0)q. \tag{27}$$

C. Simulations and discussions

In our Monte Carlo simulations, the system length $L = 500$, and system evolutes 10^6 Monte Carlo time steps (MCSs). Simulations show that the dynamical properties of the two lanes are the same, so we only carry out calculations and investigation for lane 1.

The calculation results of current are shown in Fig. 5. It can be seen that the SMF result is in good approximation with simulation result only for large values of p and q, and SMF result deviates from the simulation result generally due to stronger correlations. But it is nice to see that the CMF result is good. The CMF result is in good agreement with the simulation result for a large value of q with a fixed value of p [see Fig. 5(a)], and there are some fluctuations between the CMF result and the simulation result for a small value of q with the same p [see Fig. 5(b)]. In order to investigate in approximation the effect of mean-field analysis, contours of current deviation of mean-field analysis from the simulation drawn in (p, q) space are shown in Fig. 6. Figures 6(a) and 6(b) correspond to the deviation from SMF, and (c) and (d) correspond to the deviation from CMF. Here two deviation measures are employed: one is maximum deviation—corresponding results are shown in Figs. 6(a) and 6(c); the other is mean square deviation (standard deviation)—corresponding results are shown in Figs. 6(b) and 6(d). Here the step of density is taken as 0.05 in calculating the deviation. Based on the contour maps of the current deviate, one can note that the CMF result is much better than the SMF result; it agrees with simulation well in most areas of (p, q) space.

Additionally, Fig. 5 also shows that two maxima (double-peaked) can appear in the current-density relation, which is similar to the Katz, Lebowitz, and Spohn model [7,29]. The phase diagram for the single-peaked and double-peaked current-density relation is shown in Fig. 7. In order to analyze the appearance of these two phases, the flow rate J can be divided into four parts corresponding to four cases of model

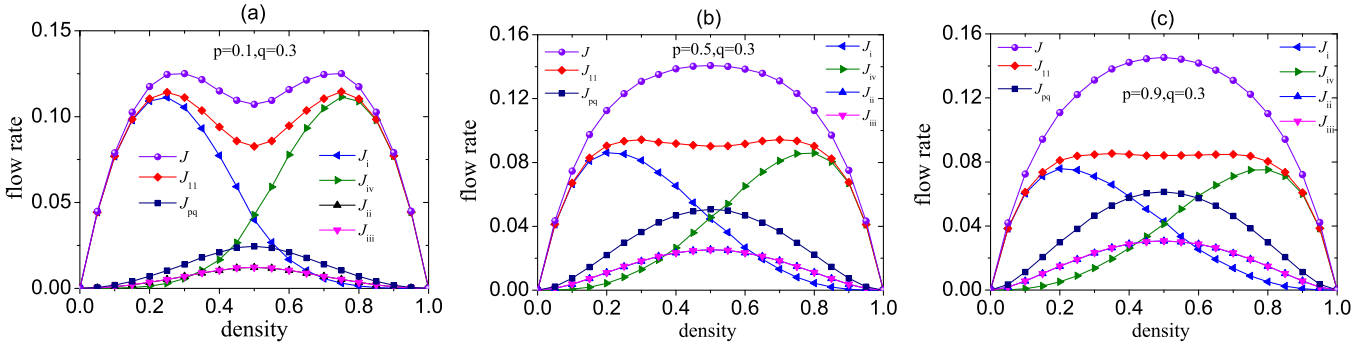

FIG. 8. Diagrams of various types current vs density ρ for (a) $p = 0.1, q = 0.3$, (b) $p = 0.5, q = 0.3$, and (c) $p = 0.9, q = 0.3$.

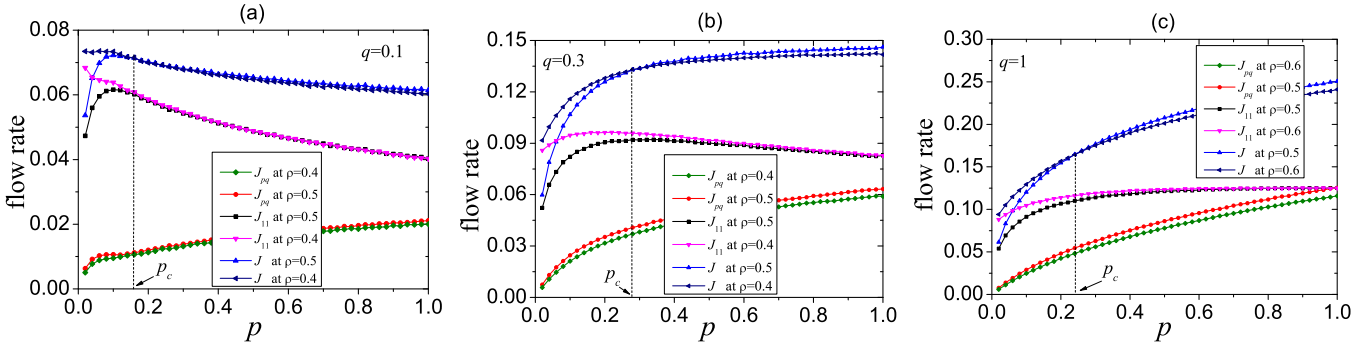

FIG. 9. Diagrams of three types of current vs p at $\rho = 0.4$ and $\rho = 0.5$ for (a) $q = 0.1$, (a) $q = 0.3$, and (c) $q = 1$. The p_c presents critical value of p from double-peaked phase to single-peaked phase corresponding to the phase boundary from simulations in Fig. 7.

rules as shown in Fig. 1. That is to say,

$$J = J_i + J_{ii} + J_{iii} + J_{iv}, \tag{28}$$

where

$$J_i = 1P(1,0), \tag{29}$$

$$J_{ii} = pP(1,2), \tag{30}$$

$$J_{iii} = qP(3,0), \tag{31}$$

$$J_{iv} = 1P(3,2). \tag{32}$$

Additionally, the sum of J_i and J_{iv} is written as J_{11} and the sum of J_{ii} and J_{iii} is written as J_{pq}, namely, $J_{11} = J_i + J_{iv}$ and $J_{pq} = J_{ii} + J_{iii}$. By simulations, Fig. 8 shows the diagrams of J_i, J_{ii}, J_{iii}, J_{iv}, J_{11}, J_{pq}, and J with $p = 0.1, q = 0.3$ and $p = 0.5, q = 0.3$. One can note that the curve of J_{11} is double peaked whether J is double peaked [Fig. 8(a)] or single peaked [Figs. 8(b) and 8(c)]. Obviously, if $\rho = 0.5$ is the minimum value point of J, flow rate J is double peaked; contrarily, if $\rho = 0.5$ is the maximum value point of J, the flow rate J is single peaked. So the investigation can be done only in the neighborhood of $\rho = 0.5$. Here $\rho = 0.4$ or $\rho = 0.6$ is taken as a representative. One can fix q, let p increase gradually, and compute flow rate J, J_{11}, J_{pq} at $\rho = 0.5$, $\rho = 0.4$, or $\rho = 0.6$. As shown in Fig. 9, when p is small, J_{11} at $\rho = 0.5$ is smaller than that at $\rho = 0.4$ or $\rho = 0.6$, and they approach gradually with the increase of p. But J_{pq} at $\rho = 0.5$ is bigger than that at $\rho = 0.4$ or $\rho = 0.6$ for arbitrary p. As a result, the total flow rate J that is the sum of J_{11} and J_{pq} at $\rho = 0.5$ can exceed that flow rate J at $\rho = 0.4$ or $\rho = 0.6$ when p is greater than the critical value p_c. It indicates that $\rho = 0.5$ is the minimum value point of J when $p < p_c$, and $\rho = 0.5$ is the maximum value point of J when $p > p_c$. Thus J changes into single peaked from double peaked with the increase of p.

In addition, one also notes that two curves of J_i and J_{iv} appear in a certain symmetry in Fig. 8. In fact, according to the particle-hole symmetry, case (i) is equivalent to case (iv) when particle and hole are exchanged. Figure 8 also shows that $J_{ii} = J_{iii}$, which can be proved as follows. Considering the temporal evolution of two-cluster probability $P(3,0)$, one can have the equation $\frac{dP(3,0)}{dt} = pP(1,2) - qP(3,0)$. When the system reaches stationary state, $\frac{dP(3,0)}{dt} = 0$. Thus $pP(1,2) = qP(3,0)$, that is to say, $J_{ii} = J_{iii}$.

To investigate deeply the mechanism causing current deviation of mean-field analysis from simulation, we explore the coarsening process of the system based on Monte Carlo simulation. To this end, we define a cluster of size s as s particles connected by each other, then discuss the normalized residence distribution, $p(s)$, which is the probability that a randomly chosen particle belongs to a cluster of size s. For a homogeneous state, $p(s)$ is monotonically decreasing. In contrast, for a jammed system, it is nonmonotonically decreasing with two distinct peaks [30]. This coarsening

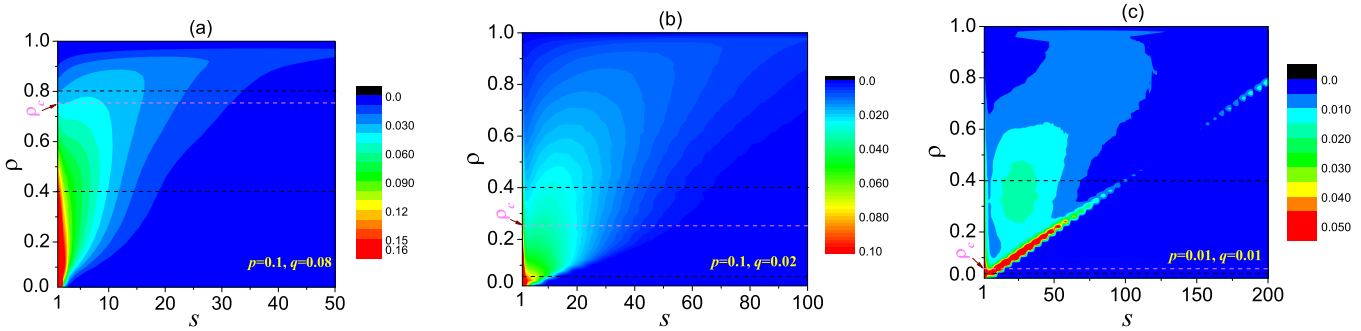

FIG. 10. Contour of normalized residence distribution $p(s, \rho)$ at (a) $p = 0.1, q = 0.08$, (b) $p = 0.1, q = 0.02$, and (c) $p = 0.01$, $q = 0.01$. The dashed line is a guide for eyes to see transformation trend of $p(s)$ at fixed ρ.

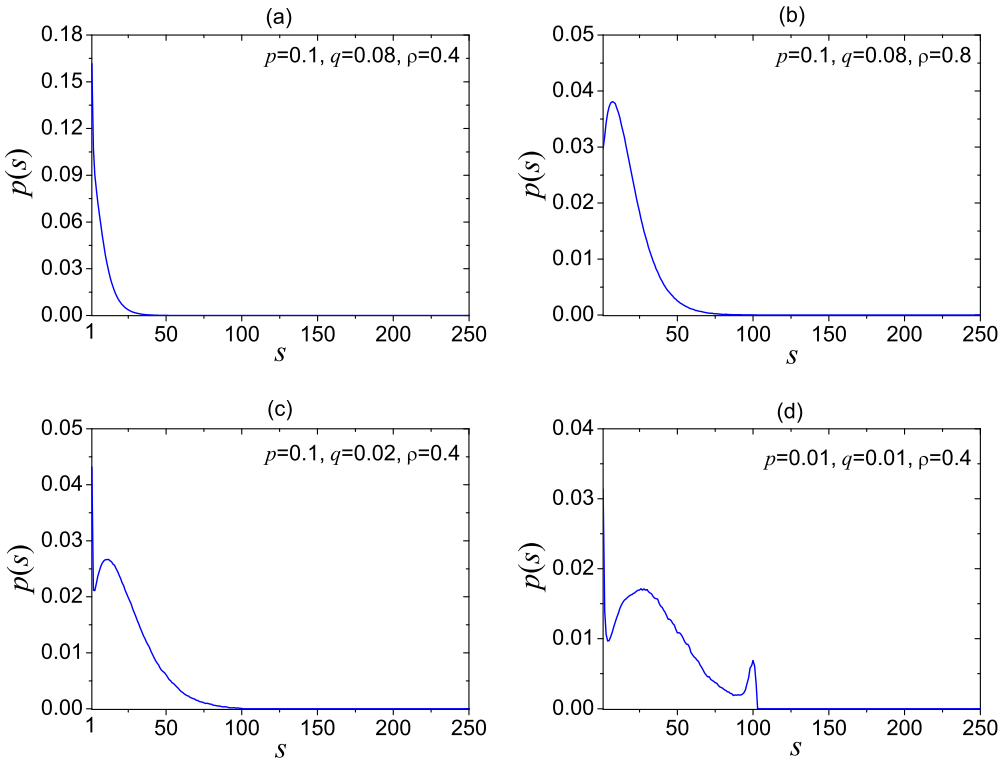

FIG. 11. Plots of normalized residence distribution $p(s)$ vs s at (a) $p = 0.1, q = 0.08, \rho = 0.4$, (b) $p = 0.1, q = 0.08, \rho = 0.8$, (c) $p = 0.1, q = 0.02, \rho = 0.4$, and (d) $p = 0.01, q = 0.01, \rho = 0.4$.

process in local domains may result in the macroscopic phase separation phenomenon eventually in some systems. In our simulations, we find that there exists a critical density ρ_c for given p and q as shown in Fig. 10. When $\rho < \rho_c$, $p(s)$ is monotonically decreasing [see Fig. 11(a)]. When $\rho > \rho_c$, $p(s)$ is nonmonotonic [see Figs. 11(b)–11(d)].

In fact, the critical density ρ_c is a function of p and q. Figure 12 presents the contour of function $\rho_c(p, q)$. One can note that values of ρ_c can be divided into roughly three intervals, $\rho_c < 0.5$, $\rho_c = 0.5$, and $\rho_c > 0.5$. When the value of q is small as shown in region I of Fig. 12, $\rho_c < 0.5$. With the increase of q as shown in region II of Fig. 12, $\rho_c > 0.5$.

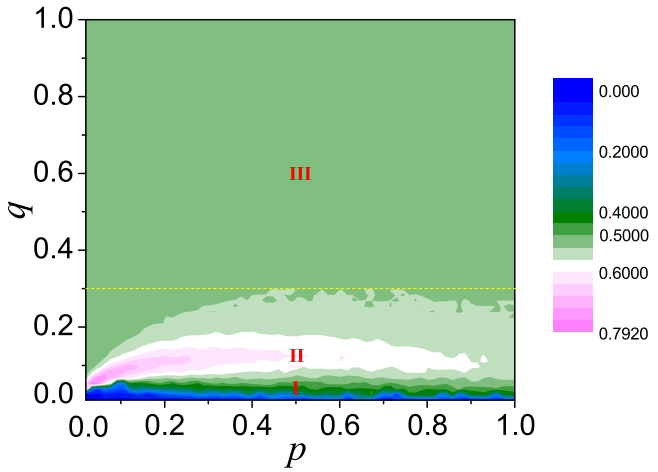

FIG. 12. Contour of critical density $\rho_c(p, q)$.

For large values of q as shown in region III of Fig. 12, $\rho_c = 0.5$. By simulation and investigation, one can speculate that the system is homogeneous when $\rho_c = 0.5$, otherwise, the system is macroscopic or microscopic inhomogeneous. First, the spatiotemporal diagram can demonstrate the above conclusion. As shown in Figs. 13(a), 13(b) 13(d), and 13(e), whether at low density or at high density, the system is in an inhomogeneous state when q is small, which is out of the range of $\rho_c = 0.5$ and corresponds to regions I and II in Fig. 12, and Figs. 13(c) and 13(f) show the system becomes a homogeneous state when q is in the range of $\rho_c = 0.5$, which corresponds to region III in Fig. 12. Second, the mean value and standard deviation of cluster size s as shown in Table I also verifies that. With the increase of q, the mean value and standard deviation of cluster size s decrease. The data for $p = 1, q = 1$ are referenced in the table, because the model with $p = 1, q = 1$ is the original TASEP model, which is homogeneous. It indicates the system becomes homogeneous from the macroscopic or microscopic inhomogeneous state with the increase of q.

Interestingly, comparing Fig. 12 with Figs. 6(c) or 6(d), one can note that the CMF result is in good agreement with simulation result around region III of Fig. 12 corresponding $\rho_c = 0.5$, and the CMF result deviates from the simulation result around regions I and II of Fig. 12 corresponding to $\rho_c > 0.5$ or $\rho_c < 0.5$. This can also confirm the conjecture that the system is homogeneous when $\rho_c = 0.5$, otherwise, the system is macroscopic or microscopic inhomogeneous. Meanwhile, it indicates that deviation of mean-field analysis from simulation is due to the inhomogeneity of the system.

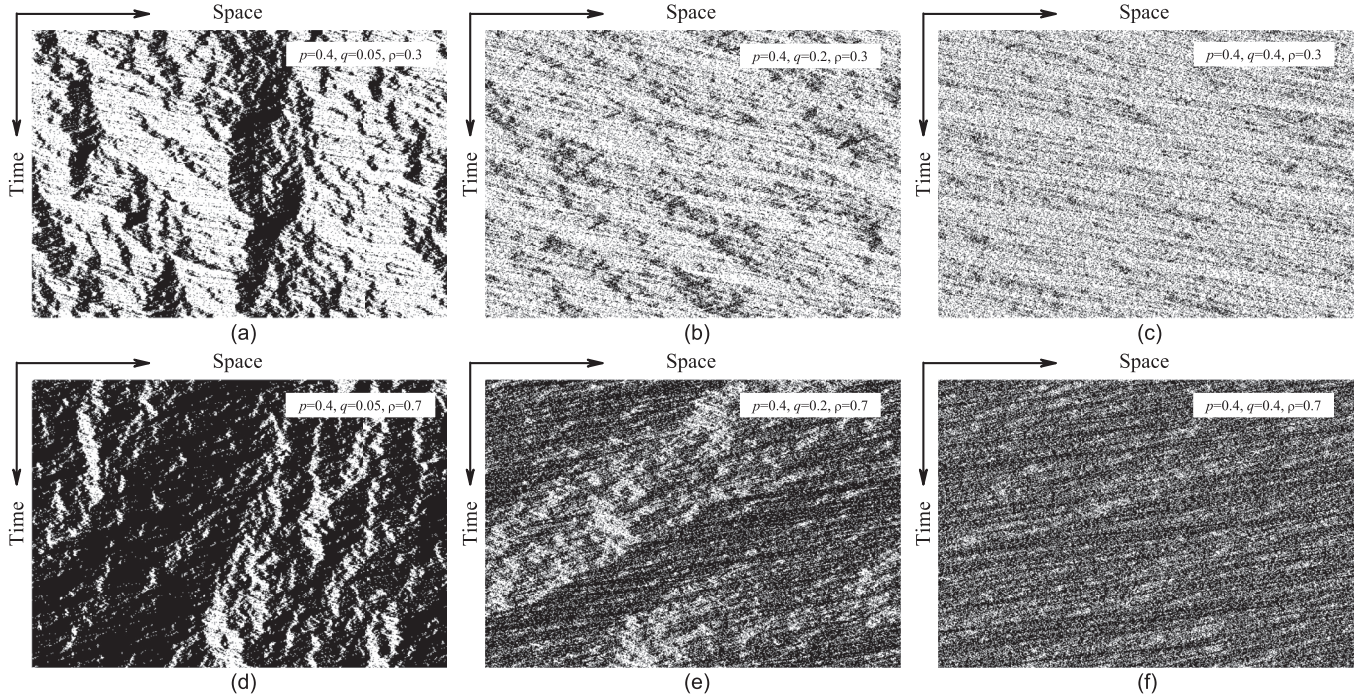

FIG. 13. Spatiotemporal diagram. (a), (b), (d), and (e) are inhomogeneous states corresponding to regions I and II in Fig. 12, (c) and (f) are macroscopic homogeneous states corresponding to region III in Fig. 12. The parameters are $p = 0.4, q = 0.05, \rho = 0.3$ in (a), $p = 0.4$, $q = 0.2, \rho = 0.3$ in (b), $p = 0.4, q = 0.4, \rho = 0.3$ in (c), $p = 0.4, q = 0.05, \rho = 0.7$ in (d), $p = 0.4, q = 0.2, \rho = 0.7$ in (e), and $p = 0.4$, $q = 0.4, \rho = 0.7$ in (f). 500 snapshots of the system are shown every 20 MCSs after 5×10^4 time steps are discarded.

IV. CONCLUSION

To summarize, this paper has presented a driven diffusive two-lane model. The dynamic characteristics under periodic boundaries are discussed by simulations and mean-field analysis methods. Simple mean-field and cluster mean-field methods are employed to calculate the flow rate. In most of the region of (p, q) space, two-cluster mean-field (CMF) results are in good agreement with simulation results. There are two types of phases about the flow rate curve: double peaked and singe peaked. Through investigating the coarsening process of the system based on Monte Carlo simulation, we find that the normalized residence distribution $p(s)$ is monotonically decreasing under the critical density ρ_c, and $p(s)$ is nonmonotonic above the ρ_c. Moreover, ρ_c is different for different parameter values of p and q. We present a conjecture that the system is homogeneous when the critical density $\rho_c = 0.5$, so in this case, CMF results are in good agreement with simulation results.

TABLE I. Mean value and standard deviation of cluster size s with $p = 0.4$ and different values of q.

	$\rho = 0.3$		$\rho = 0.7$	
q	Mean value	Standard deviation	Mean value	Standard deviation
0.05	7.12	6.08	16.29	12.03
0.2	2.73	2.10	7.60	5.46
0.4	2.00	1.29	5.88	4.01
$p = 1, q = 1$	1.85	1.10	5.62	3.90

ACKNOWLEDGMENTS

This work was funded by the National Natural Science Foundation of China (Grants No. 71621001 and No. 11475003), the Key Project of Natural Science Research in the University of Anhui Province (Grants No. KJ2017A361 and No. KJ2014A139), and the Outstanding Young Talent Support Program in the University of Anhui Province in 2014. Part of the computations have been done on the supercomputing system in the Supercomputing Center of the University of Science and Technology of China.

APPENDIX

In this Appendix, we present the other independent master equations for two-cluster probabilities under periodic boundary. The derivation method of the seven master equations is similar to that of Eq. (17). Therefore, here we only give the result ignoring the derivation process.

Considering the temporal evolution of the two-cluster probability $P(1,0)$, we can obtain

$$\frac{P(1,0)P(0,0)+P(3,0)P(0,0)q}{P(0,0)+P(1,0)+P(2,0)+P(3,0)}+\frac{P(1,1)P(1,0)+P(1,1)P(1,2)p}{P(1,0)+P(1,1)+P(1,2)+P(1,3)}$$
$$+\frac{P(1,2)P(2,0)+P(1,2)P(2,1)p}{P(2,0)+P(2,1)+P(2,2)+P(2,3)}-P(1,0)-\frac{P(3,1)P(1,0)+P(2,1)P(1,0)p}{P(0,1)+P(1,1)+P(2,1)+P(3,1)}=0. \tag{A1}$$

Considering the temporal evolution of $P(0,1)$, we can obtain

$$P(1,0)+\frac{P(0,3)P(3,1)+P(0,3)P(3,0)q}{P(3,0)+P(3,1)+P(3,2)+P(3,3)}-\frac{P(0,1)P(1,0)+P(0,1)P(1,2)p}{P(1,0)+P(1,1)+P(1,2)+P(1,3)}$$
$$-\frac{P(1,0)P(0,1)+P(2,0)P(0,1)+2P(3,0)P(0,1)q}{P(0,0)+P(1,0)+P(2,0)+P(3,0)}=0. \tag{A2}$$

Considering the temporal evolution of $P(3,0)$, we can get

$$\frac{P(2,1)P(1,0)p+P(3,1)P(1,0)}{P(0,1)+P(1,1)+P(2,1)+P(3,1)}+\frac{P(1,2)P(2,0)p+P(3,2)P(2,0)}{P(0,2)+P(1,2)+P(2,2)+P(3,2)}$$
$$+\frac{P(3,1)P(1,2)p+P(3,1)P(1,0)}{P(1,0)+P(1,1)+P(1,2)+P(1,3)}+\frac{P(3,2)P(2,1)p+P(3,2)P(2,0)}{P(2,0)+P(2,1)+P(2,2)+P(2,3)}-2P(3,0)q=0. \tag{A3}$$

Considering the temporal evolution of $P(1,2)$, we can have

$$\frac{P(3,0)P(0,2)q+P(1,0)P(0,2)}{P(0,0)+P(1,0)+P(2,0)+P(3,0)}+\frac{P(1,3)P(3,0)q+P(1,3)P(3,2)}{P(3,0)+P(3,1)+P(3,2)+P(3,3)}+P(3,0)q$$
$$-\frac{P(2,1)P(1,2)p+P(3,1)P(1,2)}{P(0,1)+P(1,1)+P(2,1)+P(3,1)}-\frac{P(1,2)P(2,1)p+P(1,2)P(2,0)}{P(2,0)+P(2,1)+P(2,2)+P(2,3)}-P(1,2)p=0. \tag{A4}$$

Considering the temporal evolution of $P(0,3)$, we can obtain

$$P(1,2)p+P(2,1)p-\frac{2P(3,0)P(0,3)q+P(1,0)P(0,3)+P(2,0)P(0,3)}{P(0,0)+P(1,0)+P(2,0)+P(3,0)}$$
$$-\frac{2P(0,3)P(3,0)q+P(0,3)P(3,1)+P(0,3)P(3,2)}{P(3,0)+P(3,1)+P(3,2)+P(3,3)}=0. \tag{A5}$$

Considering the temporal evolution of $P(3,1)$, we can obtain

$$\frac{P(1,2)P(2,1)p+P(3,2)P(2,1)}{P(0,2)+P(1,2)+P(2,2)+P(3,2)}+\frac{P(2,1)P(1,1)p+P(3,1)P(1,1)}{P(0,1)+P(1,1)+P(2,1)+P(3,1)}$$
$$+\frac{P(3,3)P(3,0)q+P(3,3)P(3,1)}{P(3,0)+P(3,1)+P(3,2)+P(3,3)}-\frac{P(3,1)P(1,2)p+P(3,1)P(1,0)}{P(1,0)+P(1,1)+P(1,2)+P(1,3)}-P(3,1)=0. \tag{A6}$$

Considering the temporal evolution of $P(1,3)$, we can obtain

$$P(3,1)+\frac{P(3,0)P(0,3)q+P(1,0)P(0,3)}{P(0,0)+P(1,0)+P(2,0)+P(3,0)}-\frac{P(2,1)P(1,3)p+P(3,1)P(1,3)}{P(0,1)+P(1,1)+P(2,1)+P(3,1)}$$
$$-\frac{2P(1,3)P(3,0)q+P(1,3)P(3,1)+P(1,3)P(3,2)}{P(3,0)+P(3,1)+P(3,2)+P(3,3)}=0. \tag{A7}$$

[1] G. M. Schütz, in *Phase Transitions and Critical Phenomena*, edited by C. Domb and J. Lebowitz (Academic Press, London, 2001), Vol. 19, pp. 1–251.

[2] N. Hirokawa, Science **279**, 519 (1998).

[3] I. Neri, N. Kern, and A. Parmeggiani, Phys. Rev. Lett. **110**, 098102 (2013).

[4] D. E. Wolf and L. H. Tang, Phys. Rev. Lett. **65**, 1591 (1990).

[5] G. M. Schütz, Europhys. Lett. **48**, 623 (1999).

[6] T. Chou, Phys. Rev. Lett. **80**, 85 (1998).

[7] S. Katz, J. L. Lebowitz, and H. Spohn, J. Stat. Phys. **34**, 497 (1984).

[8] D. Chowdhury, L. Santen, and A. Schadschneider, Phys. Rep. **329**, 199 (2000).

[9] T. Chou, K. Mallick, R. K. P. Zia, Rep. Prog. Phys. **74**, 116601 (2011).

[10] B. Mishra and D. Chowdhury, Phys. Rev. E **95**, 062117 (2017).

[11] C. T. Macdonald, J. H. Gibbs, and A. C. Pipkin, Biopolymers **6**, 1 (1968).

[12] C. T. Macdonald and J. H. Gibbs, Biopolymers **7**, 707 (1969).

[13] M. Z. Liu, S. D. Li, and R. L. Wang, Chin. Phys. B **21**, 090510 (2012).

[14] A. K. Verma, A. K. Gupta, and I. Dhiman, Europhys. Lett. **112**, 30008 (2015).
[15] I. Dhiman and A. K. Gupta, Phys. Lett. A **380**, 2038 (2016).
[16] Z. P. Cai, Y. M. Yuan, R. Jiang, M. B. Hu, Q. S. Wu, and Y. H. Wu, J. Stat. Mech. (2008) P07016.
[17] Y. Q. Wang, R. Jiang, and Q. S. Wu, Nonlinear Dyn. **88**, 1631 (2017).
[18] S. Klumpp and R. Lipowsky, Europhys. Lett. **66**, 90 (2004).
[19] H. Teimouri, A. B. Kolomeisky, and K. Mehrabiani, J. Phys. A: Math. Theor. **48**, 065001 (2015).
[20] D. Celis-Garza, H. Teimouri, and A. B. Kolomeisky, J. Stat. Mech. (2015) P04013.
[21] R. Jiang, K. Nishinari, M. B. Hu, Y. H. Wu, and Q. S. Wu, J. Stat. Phys. **136**, 73 (2009).
[22] T. Midha, A. K. Gupta, and A. B. Kolomeisky, J. Stat. Mech. (2017) 073202.
[23] A. Melbinger, T. Reichenbach, T. Franosch, and E. Frey, Phys. Rev. E **83**, 031923 (2011).
[24] G. H. Peng, Nonlinear Dyn. **73**, 1035 (2013).
[25] A. K. Gupta and I. Dhiman, Phys. Rev. E **89**, 022131 (2014).
[26] B. Derrida, E. Domany, and D. Mukamel, J. Stat. Phys. **69**, 667 (1992).
[27] I. Pinkoviezky and N. S. Gov, New J. Phys. **15**, 025009 (2013).
[28] Q. Y. Hao, Z. Chen, X. Y. Sun, B. B. Liu, and C. Y. Wu, Phys. Rev. E **94**, 022113 (2016).
[29] J. S. Hager, J. Krug, V. Popkov, and G. M. Schütz, Phys. Rev. E **63**, 056110 (2001).
[30] I. T. Georgiev, B. Schmittmann, and R. K. P. Zia, Phys. Rev. Lett. **94**, 115701 (2005).